The investigation of mid-layer cracks effects on the performance of bimorph piezoelectric energy harvester with silicon substrate

Asghar Jamshiddoust
Tarbiat Modares University
Amin Farrokhabadi (Amin-farrokh@modares.ac.ir)
Tarbiat Modares University

Article

Keywords: Energy Harvester, Power, Mid-layer Crack, Damage Detection, Health Monitoring, Stiffness Reduction

Posted Date: April 12th, 2022

DOI: https://doi.org/10.21203/rs.3.rs-1519661/v1

The investigation of mid-layer cracks effects on the performance of bimorph piezoelectric energy harvester with silicon substrate

Asghar Jamshiddoust[1], Amin Farrokhabadi[1*],

[1]Department of Mechanical Engineering, Tarbiat Modares University, P.O. Box 14115-177, Tehran, Iran

Abstract

Cracks are common faults in micro-electromechanical structures that affect the performance and dynamic behavior of the structure. Cracks can change the stiffness of the structure and parameters like resonance frequency, voltage and output power and after a specific time could lead to failure of that structure. Thus, diagnosis and identification the cracks in the structure will be very important. In the present study, a semi-analytical approach for the analysis of through the thickness cracks in the bimorph piezoelectric energy harvesters is proposed and both the stiffness reduction and changes in the capacitance of the structure due to through the thickness cracks are considered. From micromechanical point of view, a crack density based stress transfer method is employed for calculation of stiffness reduction due to crack formation in the middle layer. Analytical results of crack effects in mid-layer of a bimorph are derived by employing the Euler-Bernoulli beam theory assumptions and are validated via FEM. The effects of these defects on the mechanical parameters like resonance frequency, as well as electrical parameters like the output electrical power are discussed. It is observed that the presence of cracks in the mid-layer of bimorph piezoelectric energy harvester causes the decrease in its resonance frequency and the increase in the voltage and output power which is a sign of device failure. This work will provide an easy way for MEMS users to know some kinds of defects just only by monitoring the performance of the harvester.

Keywords: Energy Harvester, Power, Mid-layer Crack, Damage Detection, Health Monitoring, Stiffness Reduction.

1- Introduction

Supporting low power applications such as wireless sensor networks, medical devices, tire motion, robotics and self-powered autonomous systems using the energy available in their environment especially vibrational energy has attracted great attention in recent years. This demand motivated researchers towards designing energy harvesters. For this purpose, many of them focused on vibrational energy harvesting with piezoelectric materials due to their favorable frequency response and high efficiency [1-5].

* Corresponding Author: Amin-farrokh@modares.ac.ir

The layered structure with a concentrated mass at the tip of the beam is studied and it is found that decreasing the thickness of the piezoelectric layer and increasing the mass at the tip of the beam, decreases the resonance frequency and the output power would be increased by this reduction [6]. Variation of the output power with the length and width of the mass is studied by Anderson and Sexton [7]. Some research showed that employing a proof mass at the tip of the harvester would cause to have an acceptable accuracy when using single-degree-of-freedom (SDOF) model and the vibration of system is near one of its resonance frequencies. Also Erturk and Inman and Abdelkefi et al. [8-9], proposed employing an end tip mass for the moving the natural frequencies of the system to the operational frequency of the vibration source. Bai et al. [10] investigated the energy harvesting due to human motion using a cantilever structured piezoelectric energy harvester with random vibration input. For this purpose, three different conceptual designs of bimorphs were simulated with ANSYS to predict the performance and optimization of system parameters. In another attempt, using the analytical modeling, the validation of multi-mode piezoelectric energy harvester is done by Li et al. [11]. The structure configured for generating closed multiple resonance peaks within a frequency range, making it suitable for broadband energy harvesting. The validation is done through ANSYS simulations.

Piezoelectric ceramics are very brittle and susceptible to fracture which in some cases occurs by interfaces cracks or through the thickness cracks. These cracks cause to an undesired degradation of electrical and mechanical performance. Due to the increasing usage of the piezoelectric smart devices the risks that lead to multiple failures and the issues related to the failure of piezoelectric materials have attracted the attention of many researchers in recent years [12]. Also, since one application of the piezoelectric components is the failure investigation and health monitoring of other structures [13-15], it is necessary to know the signs of their own failures so as not to confuse with the performance changes of other structures. High levels of stresses, fatigue and repetitive manufacturing processes, are the major factors which can cause initiation and growth of the cracks inside the structures. The continuous growth of cracks and reaching the critical size can eventually cause sudden failure of the MEMS device [16]. The effects of surface cracks on the dynamic behavior of a piezoelectric sensor cantilever beam has been studied by Shoaib et al. [16]. In this study, the tip displacement and output voltage of a beam with a piezoelectric layer were investigated and it was found that the presence of defined surface cracks increases the displacement and output voltage of the beam. This means that the increase in voltage is a sign of failure of the part. Due to the complexity of the physics of problem at crack levels, special methods are used to model the simplified and limited types and cases [17]. Interlayer cracks have been investigated for both cracks parallel to

polarization axis and perpendicular to the polarization axis [18]. It has been shown that in bilayers that have a certain symmetry, the cracks between the bilayers do not exhibit oscillating behavior. Also, the electrical displacement due to the presence of cracks is constant at the crack levels and depends only on the applied stress field. The study of failures in piezoelectric materials is not limited to mechanical failures and some researches have been done on electrical failures of piezoelectric structures. The critical J integral at the onset of both fracture and breakdown have been calculated numerically via finite element analysis by Beom et al. [19]. They discussed the effects of both the direction of the electric field and the poling direction on both fracture and breakdown resistance. The fracture mechanics problem of a Griffith crack embedded in a two-dimensional magnetoelectric composite material subjected to coupling mechanical, electric and magnetic loads at infinity investigated by Zhang et al. [20]. The impact of polling direction on fracture parameters of a limited permeable interface crack in a piezoelectric bi-material is considered by Viun et al. [21].

Crack analysis in the piezoelectric material with considering the electric field and strain gradient has been done by Sladek et al. [22]. In this research the behavior of cracks in two-dimensional piezoelectric material was investigated. Periodic permeable interface cracks in piezoelectric materials were investigated by Gao et al. [23]. This work revisited the generalized 2D problem of electrically permeable collinear interface cracks in piezoelectric materials. It was shown that under the electric loading only, the electric fields are uniform not only in the materials but also inside the cracks, while the stress is zero wherever. Interface cracks in piezoelectric materials have been also discussed in several articles due to its importance [24], [25]. In these studies, the electrical field inside the crack has been analyzed and shown that it depends on the material constants as well as the applied load. Effects of crack surface electrostatic tractions on the fracture behaviour of magnetoelectric composite materials investigated by Zhang et al. [26]. They found that the electrostatic tractions on the crack surfaces have the tendency to close the crack therefore cause the retardation of the crack propagation. It was shown that the traditional traction-free crack model always overestimates the effect of applied magnetoelectric loads on the crack tip filed intensity factors. Finally, Ayatollahi et al. [27] studied the multiple interfacial cracks in dissimilar piezoelectric layers under time harmonic loadings. Straight and sharp cracks have been observed and reported in silicon 100 [28]. It was observed that, the increase in crack length depends on the crystal coordinates of the structure. These direct cracks which propagate in the 100 and 110 directions could also be observed due to fatigue loading [29].

Silicon, the most common single material used in microelectromechanical systems, is an inhomogeneous crystalline material whose properties depend on the positional coordinates relative to the crystal lattice. Due to the complexity of the subject, many researchers have used inaccurate values for design and analysis by simplifying the elastic properties of silicon. Estimations with isotropic consideration of silicon are mainly done in the initial design calculations [30]. Reviewing the beforementioned studies and according to the author's knowledge, no comprehensive study has been proposed for the analysis of crack effects in the mid-layer of piezoelectric energy harvesters with silicon substrate and this type of problem has not been investigated before. So this study provides a procedure for analysis of damage in the midlayer of bimorph using the simoultenous analytical and numerical studies. The details of these approches will be reported in the following sections.

2- Piezoelectric Energy Harvesting System Model

In this section, the equations of a bimorph with silicon substrate will be developed. The silicon 100 with anisotropic properties is used as substrate between two layers of PZT. The energy harvester system in this study is a piezoelectric beam that is shown in Fig 1. The structure is a composite cantilever beam consisting of three layers with a proof mass at the free end which is used for adjusting the natural frequency. The length to thickness ratio of the beam is large enough to satisfy the Euler-Bernoulli beam theory. As it can be seen in Figure 1, h_p and h_s are the thickness of the piezoelectric and substrate layer respectively, q is the tip displacement, and $u(t)$ is harmonic excitation displacement.

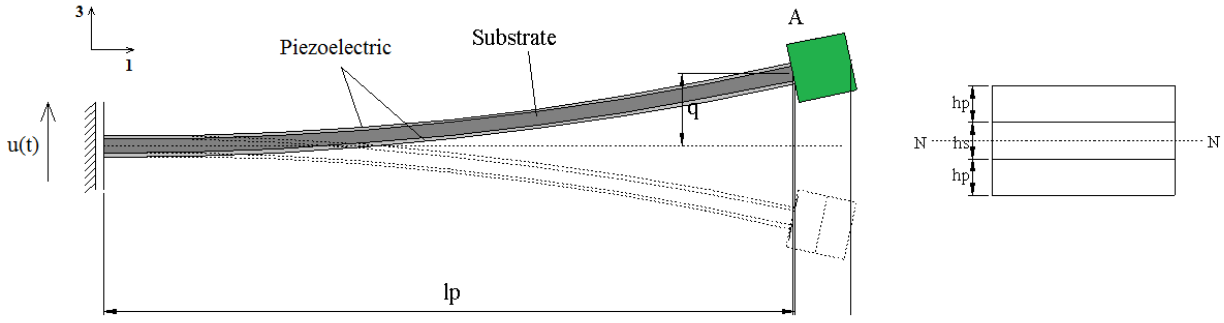

Fig 1. Piezoelectric energy harvester and cross-sectional view.

2-1- Governing Equations

One end of the bimorph which is shown in Fig 1 is cantilevered into the wall and vibrates harmonically along the vertical direction. A mass m_0 is connected to the end of bimorph for adjusting the vibration characteristics of the beam. The electrodes at the bottom and top surfaces of the bimorph can be wired as a parallel connection or serial connection. Poling the piezoelectric layers in the same direction, would cause to produce electric fields in opposite directions. In addition poling the piezoelectric layers in the opposite direction would cause to produce electric fields in same directions. These connection types are serial and parallel, respectively.

The excitation of the structure is done by an external harmonic displacement and is expressed as

$$u(t) = u_0 \exp(i\omega t) \tag{1}$$

Where u_0 is the amplitude of the displacement excitation and ω is the excitation frequency. The reduced form of piezoelectric constitutive equations for calculation of the axial stress and the transvers electric displacement can be written as [31]

$$S_1 = c_{11}^{-1} T_1 + d_{31} E_3 \tag{2}$$

$$D_3 = d_{31} T_1 + \varepsilon_{33} E_3 \tag{3}$$

Where c_{11}^E is the axial elastic stiffness at constant electric field, e_{31} is the piezoelectric stress coefficient, d_{31} is the transverse-axial piezoelectric constant and ε_{33} is the permittivity under constant strain. Regarding the linear analysis of the structure, the constant damping ratio option is used which is applicable to linear analysis. Damping of piezoelectric ceramics is often considered by assuming complex values for the elastic constants, and thus, in the numerical calculations, the axial elastic compliance s_{11}^E is replaced by $s_{11}^E(1 - iQ^{-1})$, where Q is the quality factor of the material [31]. As a result, Eqs. (2) and (3) can be rewritten as

$$T_1 = c_{11}^E S_1 - c_{11}^E d_{31} E_3 \tag{4}$$

$$D_3 = d_{31} T_1 + \varepsilon_{33} E_3 \tag{5}$$

Substituting (4) into (5) results

$$D_3 = d_{31} c_{11}^E S_1 + E_3(\varepsilon_{33} - c_{11}^E d_{31}^2) \tag{6}$$

The capacitance of the piezoelectric, C_p can be defined as

$$C_p = \varepsilon_{33}(1 - k_{31}^2)\frac{bL}{h_p} = K_{eq}\frac{bL}{h_p} \tag{7}$$

$$k_{31} = \frac{c_{11}^E d_{31}^2}{\varepsilon_{33}} \tag{8}$$

The strain in axial direction is represented in terms of deflection $u_3(x_1, t)$ as

$$S1 = -x_3 \times u_{3,11} \tag{9}$$

In addition, the mid layer is made of silicon and its constitutive relation can be written as

$$\begin{bmatrix} T_1 \\ T_2 \\ T_{12} \end{bmatrix}_s = \begin{bmatrix} \overline{Q}_{11} & \overline{Q}_{12} & \overline{Q}_{16} \\ \overline{Q}_{16} & \overline{Q}_{22} & \overline{Q}_{26} \\ \overline{Q}_{16} & \overline{Q}_{26} & \overline{Q}_{66} \end{bmatrix}_s \begin{bmatrix} S_1 \\ S_2 \\ S_{12} \end{bmatrix}_s \tag{10}$$

Having the strain value in the silicon-made layer, the corresponding stress value can be determined from the Eq. (10) as

$$T_{1-s} = Q_{11,s} \times S_1 \tag{11}$$

Where

$$Q_{11's} = \frac{E_{11's}}{1 - \nu_{12} \times \nu_{21}} \tag{12}$$

The electric field in the piezoelectric layer regarding to the electrode configuration can be written in the following form

$$E_3 = -\frac{V(t)}{h_p} \tag{13}$$

For calculation of the bending moment, the axial stress relations in (4) and (11) can be employed as

$$M = \iint x_3 T_1 dx_2 dx_3 \tag{14}$$

$$= 2\int_0^c \int_0^b x_3 (Q_{11,s} \times S_1)(-x_3 u_{3,11}) dx_2 dx_3$$

$$+ 2\int_c^{c+h} \int_0^b x_3 [c_{11}(-x_3 u_{3,11}) - c_{11} d_{31} E_3] dx_2 dx_3$$

$$= -\frac{2}{3} b \frac{E_{11's}}{1 - \nu_{12}\nu_{21}} u_{3,11} c^3 - \frac{2b}{3} u_{3,11} c_{11} \left[(c + h_p)^3 - c^3\right]$$

$$- b c_{11} d_{31} E_3 (2c + h_p) h_p$$

Where

$c = h_s/2$

Furthermore having the bending moment, the shear force can be calculated as

$$N = \frac{dM}{dx_1} = -\frac{2}{3} b \frac{E_{11's}}{1 - \nu_{12}\nu_{21}} u_{3,111} c^3 - \frac{2b}{3} u_{3,111} c_{11} \left[(c + h_p)^3 - c^3\right] \tag{15}$$

Employing Euler-Bernoulli beam theory, the equation of motion can be written as

$$m\ddot{u}_3 = M_{,11} \tag{16}$$

Where m is linear mass density. Substituting M from (14) into (16) results

$$m\ddot{u}_3 = -\frac{2}{3} b \frac{E_{11's}}{1 - \nu_{12}\nu_{21}} u_{3,1111} c^3 - \frac{2b}{3} u_{3,1111} c_{11} \left[(c + h_p)^3 - c^3\right] \tag{17}$$

The electrical charge at the electrode of piezoelectric layer is denoted by Q_p and can be calculated as

$$Q_p = -\iint D_3\, dx_1 dx_2 \tag{18}$$
$$= -b\int_0^L d_{31}c_{11}^E(-x_3 \times u_{3,11}) + E_3(\varepsilon_{33} - c_{11}^E d_{31}^2)dx_1$$
$$= -b[d_{31}c_{11}^E(c+h_p) \times [u_{3,1}(L,t) - u_{3,1}(0,t)] + E_3(\varepsilon_{33}$$
$$- c_{11}^E d_{31}^2)\, L]$$

This electric alternating charge creates alternating current i_p at each electrode that can be obtained as

$$I_p = -\dot{Q}_p \tag{19}$$

From the calculated value for current, the output voltage can be determined as

$$V_p = 2RI_p \tag{20}$$

Where R is the resistance load.

At the left side of the beam the boundary conditions are as

$$u_3(0,t) = u_0 \exp(i\omega t) \tag{21}$$

$$u_{3,1}(0,t) = 0 \tag{22}$$

At the free end of the harvester the bending moment is zero, but there is a shear force that can be calculated as

$$M(L,t) = 0 \tag{23}$$

$$N(0,t) = -m_0 \ddot{u_3}(L,t) \tag{24}$$

By using the complex notation for the harmonic motion we have

$$\{u_3(x), V, Q_p, I\} = Re\{U(x), \bar{V}, \overline{Q_p}, \overline{I}\}\exp(i\omega t)\} \tag{25}$$

Then Eq. (16) become

$$-\omega^2 mU = M_{,11} \tag{26}$$

The general solutions of the Eq. (26) can be written as

$$U = C_1 sin\alpha x_1 + C_2 cos\alpha x_1 + C_3 sinh\alpha x_1 + C_4 cosh\alpha x_1 \tag{27}$$

By rewriting the Eqs. (21) to (24) using the complex notation and substitution of (27) into boundary conditions and voltage equation leads to 5 equations with 5 unknowns. By concurrent solving the obtained equations, the output voltage can be determined. By solving Eqs. (19) and (20), and using calculated electric current, I_p and voltage V_p , the output electrical power P can be determined as,

$$P = \frac{V_p\, I_p}{2} \tag{28}$$

2-2- Solution for harvested power

Analytical results obtained by the experimentally validated analytical method developed by Liao and Sodano [32]. Effective parameters of a symmetric bimorph beam harvester like M, K, θ, C_p, D in closed-form were given as [33],

$$M = (\rho_s t_s + 2\rho_p t_P)\, b \tag{29}$$

$$K = \left[1.0302 E_s \left(\frac{h_s^3}{L^4}\right) + 2.0604 E_p \left(\frac{3h_s^2 h_p + 6h_s h_p^2 + 4h_p^3}{L^4}\right)\right] b \tag{30}$$

$$\theta = -2.753 d_{31} E_p b \left(\frac{h_s + h_p}{\sqrt{L^3}}\right) \tag{31}$$

$$C_p = 2K_3 \varepsilon_0 b \left(\frac{L}{h_p}\right) \tag{32}$$

$$D = -0.783 b\left(\rho_s h_s + 2\rho_p h_p\right)\sqrt{L} \tag{33}$$

By using of the basic circuit theories of a system with harmonic base excitation of amplitude u_0 the extracted power in the resistive component can be calculated as [32],

$$P = \frac{D^2 u_0^2}{\sqrt{MK}} \frac{k^2 r^2 \gamma}{(2dr + (1 + k^2 - r^2) r\gamma)^2 + (1 - r^2 - 2dr^2\gamma\,)^2} \tag{34}$$

Where the dimensionless electrical resistance and reactance are defined respectively as

$$\gamma = w_n C_p R \tag{35}$$

Furthermore, the electromechanical coupling coefficient k^2 and frequency ratio are defined as follows

$$k^2 = \frac{\theta^2}{C_p K}\ , r = \frac{w}{w_n} \tag{36}$$

Where w_n is the short-circuit natural frequency.

3- Effect of through the thickness cracks in the mid-layer of piezoelectric bimorph and mechanical properties degradation analysis

Middle layer cracks affect the stress distribution and reduce the stiffness of the structure. Increasing the number of cycles can enhance the number of these cracks. While the damage in the mid-layer can lead to significant loss of material properties, however it is not obvious sometimes. If the damage of mid layer is not detected, it could lead to the failure of the system. Through the thickness cracks in the mid-layer are often the primary mode of failure and may accumulate to high densities with increasing load. These types of cracks form along the entire thickness of the layer and are almost parallel to each other.

To ensure the safe use of piezoelectric materials, it is necessary to properly understand the failure response of this type of failure. In this work, two methods including micromechanics approach and combined fracture mechanics-finite element analysis method are used for evaluating the stiffness reduction. The properties of bimorph beam energy harvester are given in Table 1.

Table 1-PZT and silicon properties

Parameters			Symbol	Value	Unit
Material	PZT-5H	Piezoelectric Capacity	C_p	83.67	nF
		Piezoelectric electromechanical coupling	d_{31}	-274×10^{-12}	C/N
		Density	ρ	7960	Kg/m^3
		Young Modulus in the longitude direction	$E_{11,p}$	37	GPa
		Young Modulus in the lateral direction	$E_{22,p}$	18.5	GPa
		Poisson's ratio	$\nu_{12} = \nu_{21}$	0.31	---
	Silicon(100) [30]	Young Modulus (x_1)	E_1	169	GPa
		Young Modulus (x_2)	E_2	169	GPa
		Young Modulus (x_3)	E_3	130	GPa
		Young Modulus (x_2x_3)	G_{23}	79.6	GPa
		Young Modulus (x_3x_1)	G_{31}	79.6	GPa
		Young Modulus (x_1x_2)	G_{12}	50.6	GPa

		Poisson's ratio (x_2x_3)	ν_{23}	0.36	---
		Poisson's ratio (x_3x_1)	ν_{31}	0.28	---
		Poisson's ratio (x_1x_2)	ν_{12}	0.064	---
		Density	ρ	2330	Kg/m^3
Physical		Resistance Load	R	175	Ohm
		Piezoelectric layer thickness	h_p	0.6	mm
		Substrate layer thickness	h_s	0.7	mm
		Permittivity	ε_0	8.854×10^{-12}	---
		Beam length	L	100	mm
		Beam width	b	10	mm
		Damping ratio (Equivalent Q value)	d	0.01 (50)	---

3-1- Stiffness reduction calculation using finite element analysis

Using the finite element analysis on the bimorph piezoelectric energy harvester containing the different number of through the thickness cracks in the mid-layer, at different applied longitudinal load, the strain energy can be evaluated as

$$SE = \frac{\sigma_1^2 V}{2 \times E_1} \tag{37}$$

Then, the axial modulus can be obtained as [34]

$$E_1 = \frac{\sigma_1^2 V}{2 \times SE} \tag{38}$$

The corresponding crack growth simulation results versus cracks number is shown in Figure 2 .

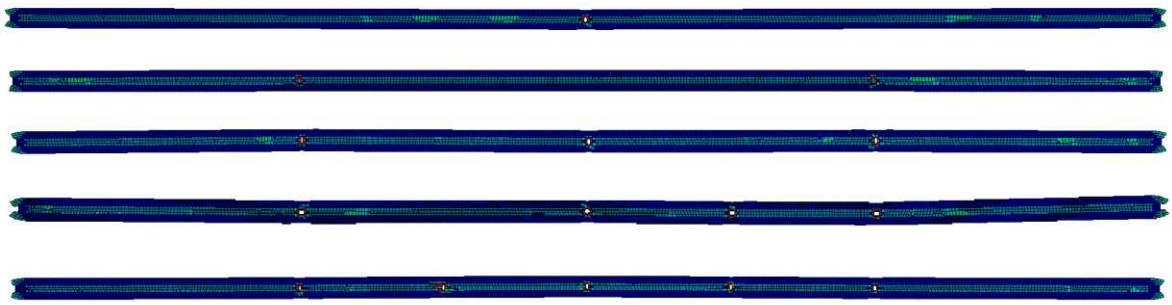

Figure 2: Effect of different Crack numbers in the mid layer form 1 crack to 5 cracks

3-2- Stiffness reduction calculation using analytical approach

To investigate the effect of mid-layer cracks on the dynamic behavior and output power of beam made of piezoelectric materials, it is possible to perform mid-layer crack analysis from a micromechanical point of view using the crack density based stress transfer method introduced by Farrokhabadi et al. [35].

This method is not limited to a specific arrangement of layers. While some methods only consider stiffness loss based on changes in crack density, using this method, a comprehensive analysis of the effect of mid-layer cracks on multilayer stiffness degradation can be obtained. In this method, the layers are considered orthotropic and the equations of equilibrium, compatibility, continuity conditions for forces and displacements, and external boundary conditions are accurately satisfied. The stiffness reduction due to crack formation in the middle layer is calculated using the micromechanics model. Using the method introduced by Farrokhabadi et al. [36], the mechanical properties of the damaged layer such as $E_1(\rho), E_2(\rho), G_{12}(\rho), \ldots$ can be obtained as a function of crack density. To do this, three independent constants like $k, k' and\ D$ are defined. Where the constants k and k' are dependents of the damage parameter. With these constants, the reduced properties of the material can be calculated as

$$\frac{\nu_{21}}{E_2} - k\frac{D(\rho)}{E_2} = \frac{\nu_{21}(\rho)}{E_2(\rho)}, D(\rho) = \frac{E_2}{E_2(\rho)} - 1, \tag{39}$$

$$\frac{\nu_{23}}{E_2} - k'\frac{D(\rho)}{E_2} = \frac{\nu_{23}(\rho)}{E_2(\rho)}, \frac{1}{E_1} - k^2\frac{D(\rho)}{E_2} = \frac{1}{E_1(\rho)}$$

$$\frac{\nu_{13}}{E_1} - kk'\frac{D(\rho)}{E_2} = \frac{\nu_{13}(\rho)}{E_1(\rho)}, \frac{1}{E_3} - k'^2\frac{D(\rho)}{E_2} = \frac{1}{E_3(\rho)}$$

In the above relation, the parameters $\mathrm{E}_1(\rho), \mathrm{E}_2(\rho), \mathrm{G}_{12}(\rho), \ldots$ are the elastic constants of damaged ply that are unknown and calculated according to the damage parameter $D(\rho)$.

4- Effect of mid-layer crack on the output electrical power

Due to the formation of through the thickness cracks in the silicon layer of a bimorph piezoelectric energy harvester, two cases may occur regarding the formation of electric field inside of these cracks. In case of an electrically impermeable crack that no electric field is created inside the crack, only the stiffness reduction affects the output electrical power and changes it. In the worst case, if the electric field forms inside the crack, in addition to stiffness reduction, the electric field inside the crack will also affect the output electrical power. For example, opening the connection or glue between the layers and assuming that the crack is extended also in the electrode section, causes the barrier between poles of different layers to be removed and the poles face each other that lead to creation of an electric field or force inside the crack section depending on the connection type whether it is parallel or serial.

Regarding the Euler-Bernoulli assumptions and due to large amount of the length to thickness ratio of the beam, the equivalent capacitor capacity of each piezoelectric layer can be calculated as

$$C = \frac{AK\varepsilon_0}{d} \tag{40}$$

Where A is the cross-sectional area of piezoelectric layers and can be used to calculate the current passing through this surface.

$$A = b \times L \tag{41}$$

$$Q_t = \sigma \times A \tag{42}$$

Also, the flux passing through the surface is calculated as

$$\sigma = \frac{Q_t}{A} = \frac{Q_{crack}}{A_{crack}} \tag{43}$$

To calculate the amount of current passing through the surface of the cracked section, in the first step, the area of its cross-sectional area is obtained and then the current passing through the surface of the cracked part can be calculated.

$$A_{crack} = b \times t_{crack} = b \times \frac{h_s}{20} \tag{44}$$

Where the crack thickness with an engineering assumption is considered as $\frac{h_s}{20}$. According to the above relations we have:

$$Q_{crack} = \frac{(h_s/20)}{L} Q_t = \frac{h_s}{20L} Q_t \tag{45}$$

The crack position in the structure can be seen in Figure 3.

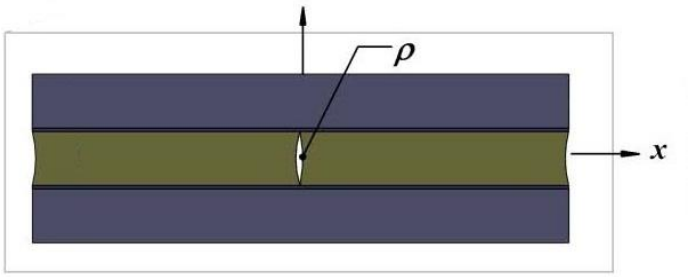

Figure 3: The crack position in the structure [32]

4-1- Crack in the mid-layer of parallel connection

In the case of a parallel connection of piezoelectric layers, an electric field is formed inside the crack of middle layer due to facing of the opposite poles each other as shown in Figure 4.

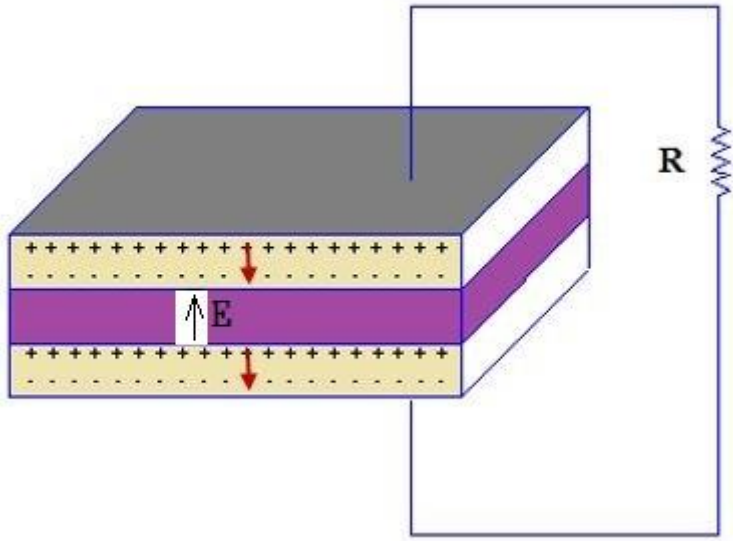

Figure 4: Electric field creation inside the middle layer in the case of crack in piezoelectric parallel connection

The equivalent circuit of the piezoelectric energy harvester will be changed as shown in Figure 5. By assuming the ideal capacitors, the equivalent capacitance of each part including piezoelectric layer and crack section, can be calculated as follows respectively [37].

$$C = \frac{bLK\varepsilon_0}{h_p} \tag{46}$$

$$C' = \frac{bh_cK'\varepsilon_0}{h_s} \tag{47}$$

In the above equation, h_c is the crack thickness, K is the dielectric coefficient in the piezoelectric material and K' is the dielectric coefficient is in the crack section which can be filled with intermediates such as air, silicone oil or water and it is desirable to consider the properties of these intermediates.

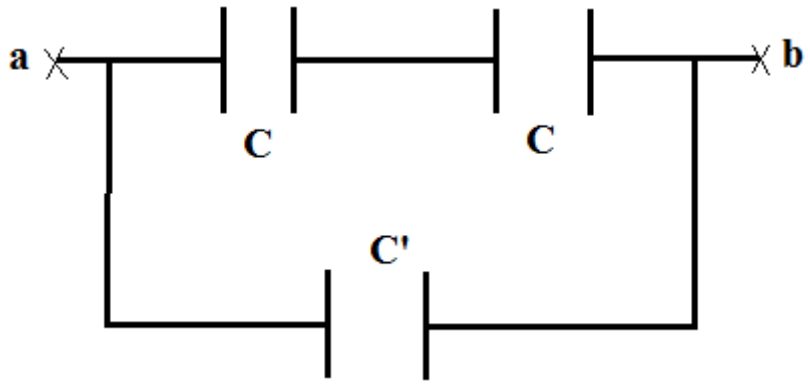

Figure 5: The piezoelectric energy harvester with crack in the mid- layer equivalent circuit in parallel connection

By increasing the cracks number in the mid-layer of bimorph the equivalent circuit changes accordingly and the equivalent capacitance of each case can be calculated.

$$C_{eq} = \frac{C}{2} + nC' \tag{48}$$

Where n is the number of cracks. Since the capacitance of each piezoelectric layer is known, the equivalent capacitance of crack section can be determined as [38]

$$\frac{C'}{C} = \frac{h_c K'}{h_s} \times \frac{h_p}{LK} \tag{49}$$

The effect of silicon layer thickness on the ratio of crack section capacitance to piezoelectric layer capacitance is shown in Figure 6 and it can be seen that the crack section capacitance is much smaller than the piezoelectric layer capacitance even in the higher value of thickness.

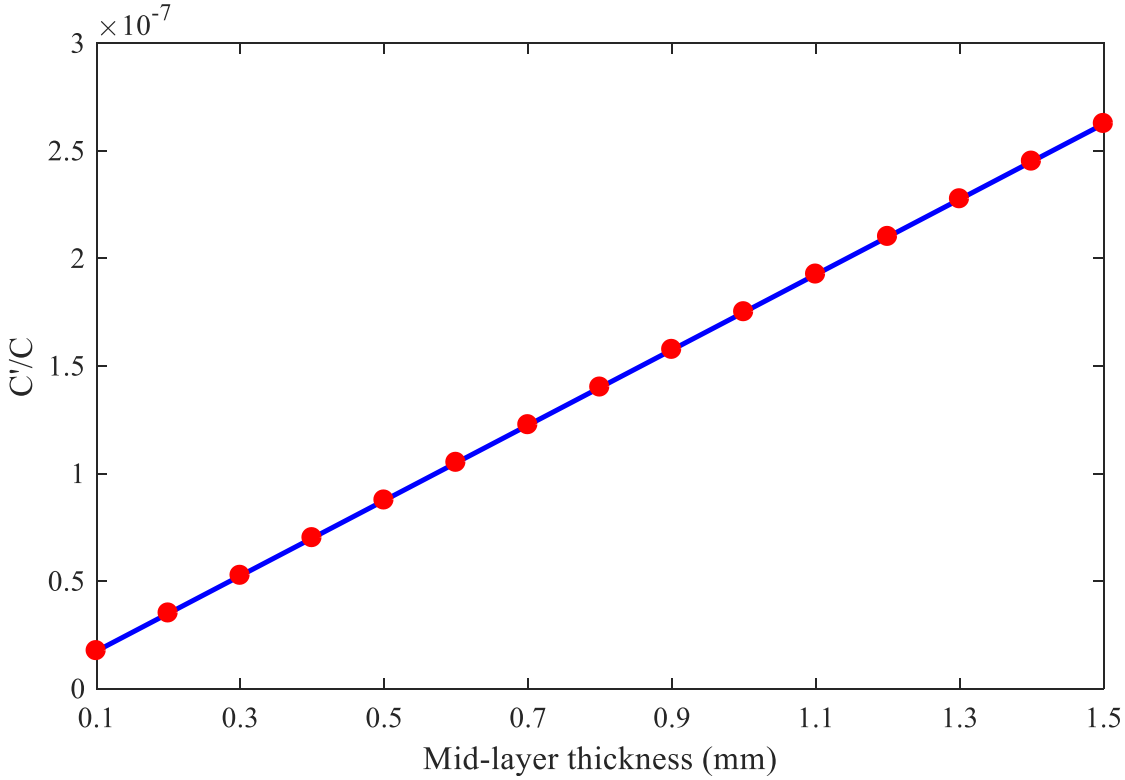

Figure 6: The ratio of crack section capacitance to piezoelectric layer capacitance

4-2- Crack in the mid-layer of serial connection

In the case of serial connection, the presence of cracks (Figure 7) causes the poles of the same name to face each other and no electric field is formed. But it causes repulsive force in this section. The formation of the force is shown in Figure 8.

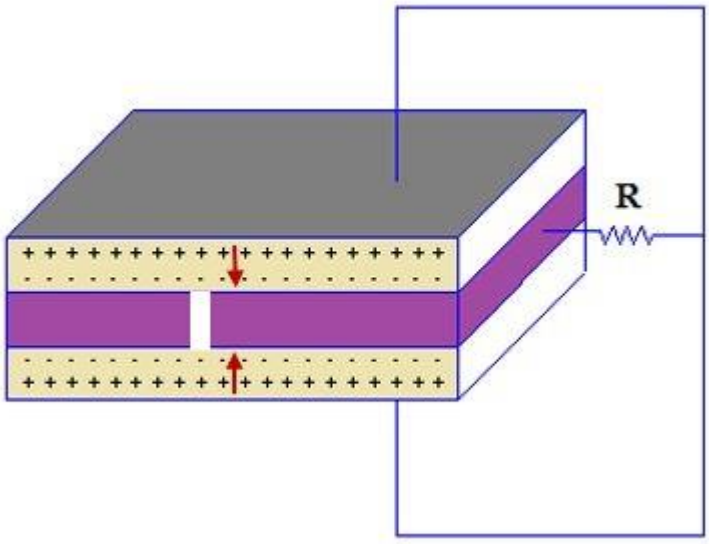

Figure 7: Repulsive force Creation inside the middle layer in the case of crack in the piezoelectric serial connection

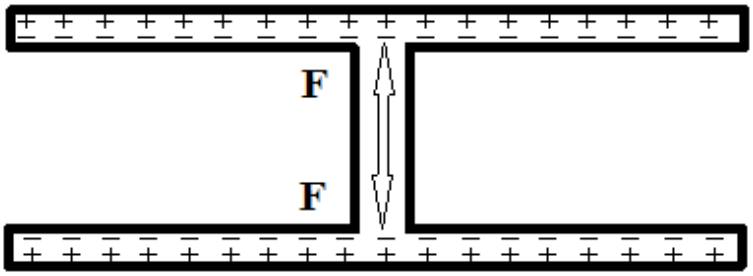

Figure 8: Formation of repulsive force at the crack site in the case of serial connection of piezoelectric layers

In this case, the capacitance in the cracked section is zero and the equivalent capacity is calculated as

$$C_{eq} = 2C \tag{50}$$

$$C_{crack} = 0 \tag{51}$$

Since the electric field does not form in the crack section of serial connection mode, similar to the impermeable cracking mode, only stiffness reduction will affect the output electrical power and the results are the same as for impermeable cracks. Then the repulsive force value can be calculated as

$$F = \frac{kQ'}{h_s^2} \tag{52}$$

5- Finite element model for the bimorph energy harvester

The finite element analysis for the bimorph energy harvester is done with ANSYS and composed of three different types of elements including 640 solid226 piezoelectric elements, 320 solid186 structural elements determined by a convergence test, and one CIRCU94 which is shown in Figure 9. The resistance between the top electrode and bottom electrode simulated by the Circuit 94 element that has two nodes and can interface with piezoelectric element. The voltage coupling between the piezoelectric layers and circuit element is represented in Figure 10.

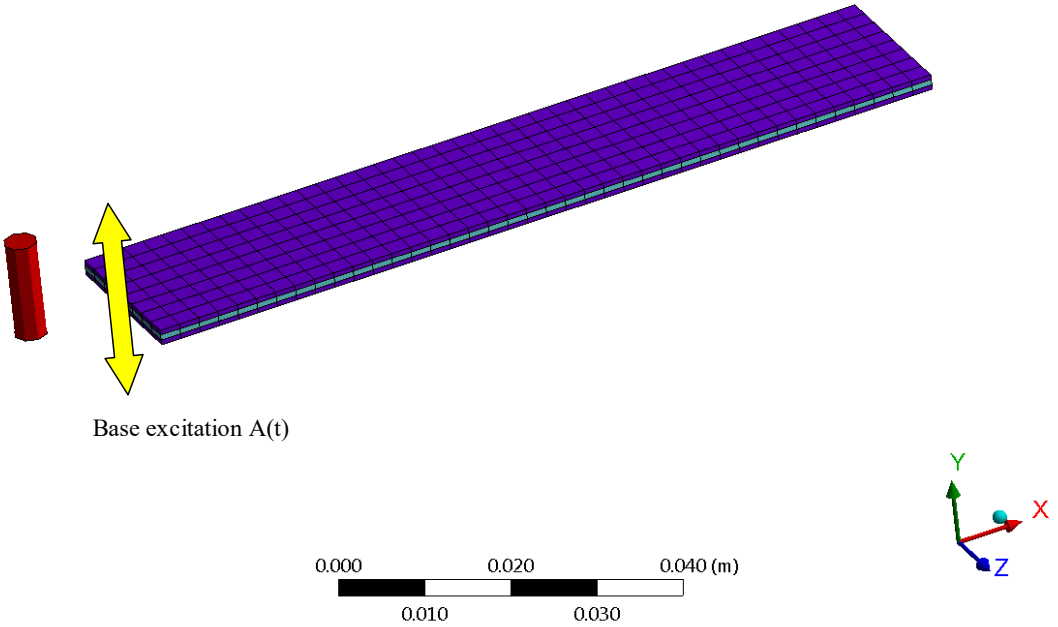

Figure 9: Finite element model of the bimorph energy harvester with external resistance in ANSYS

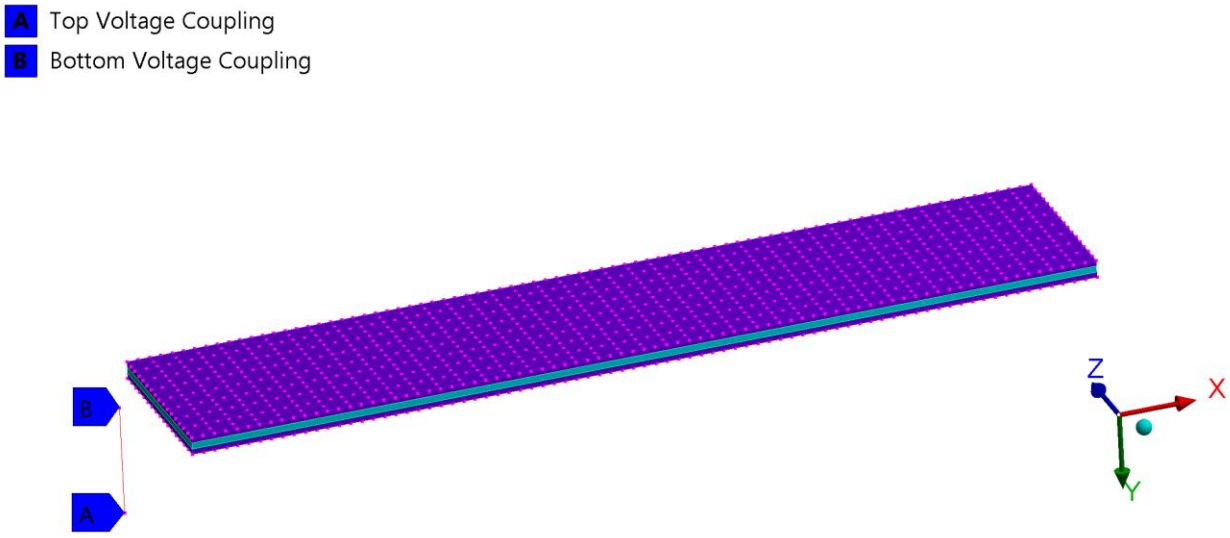

Figure 10: The voltage coupling between the piezoelectric and circuit element

6- Results and discussion

Before doing the damage analysis, the analytical solution for calculating the voltage and power is investigated. The output voltage vs. excitation frequency of the bimorph energy harvester from analytical solution and finite element analysis are shown in Figure 11.

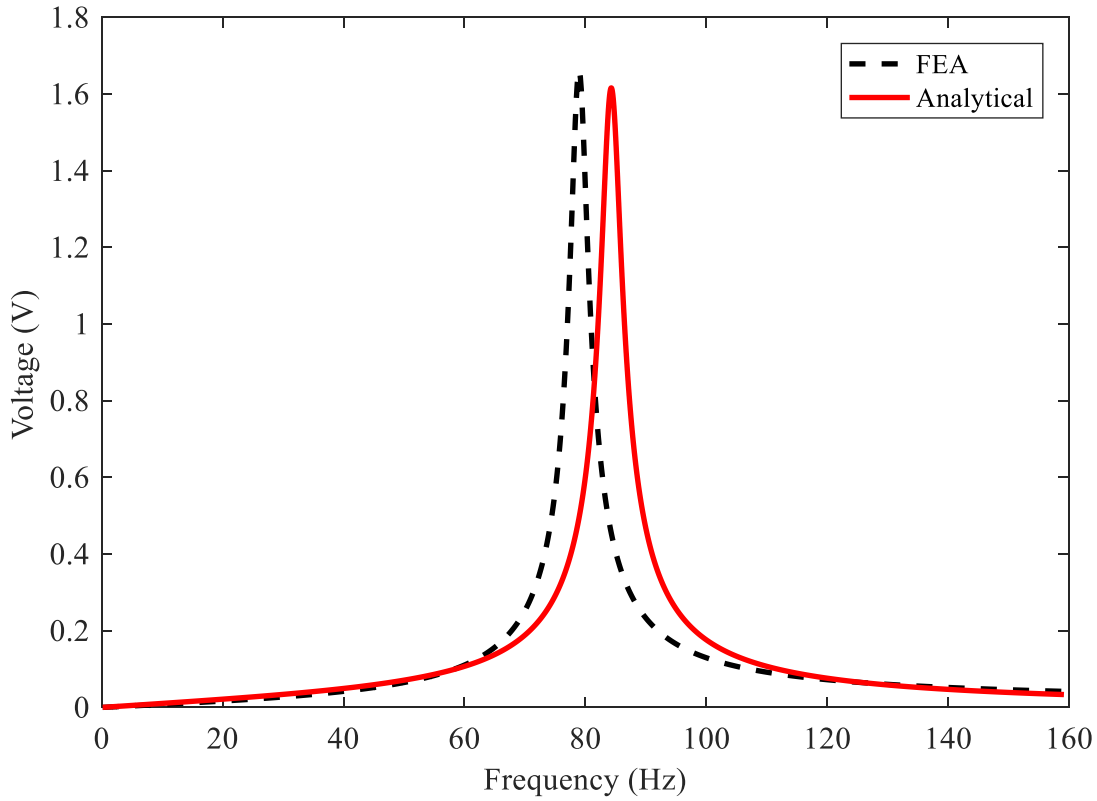

Figure 11: Output voltage of the bimorph energy harvester vs. excitation frequency from Analytical solution and FEA

The analytical solution is compared with finite element analysis and it is shown that there is a good agreement between the voltage spectrum by the analytical model and finite element results with an approximately 5.7 % difference of the resonance frequency. The analytical and FEA models predict the resonance frequency as 83.5 Hz and 78.8 Hz respectively. The small amount of difference is mainly due to the Euler-Bernoulli beam theory assumptions, while the continuous physical system is considered in the finite element analysis.

The axial stiffness of the damaged layer can be calculated according to the micromechanics approach which is shown in Table 2 for different crack numbers.

Table 2: Calculated axial stiffness of mid-layer using micromechanics approach

Case	undamaged	1 crack	2 cracks	3 cracks	4 cracks	5 cracks
Axial Stiffness (GPa)	169	163.593	158.521	153.781	149.265	145.031

Also the results of the analysis performed for the piezoelectric bimorph using this method is shown in Table 3. The axial stiffness of the damaged layer and also the bimorph beam versus number of cracks using the micromechanics approach are shown in Figure 12.

Table 3: Calculated axial stiffness of piezoelectric bimorph using micromechanics approach

Case	undamaged	1 crack	2 cracks	3 cracks	4 cracks	5 cracks
Axial Stiffness (GPa)	86.252	83.664	81.815	80.081	78.451	76.917

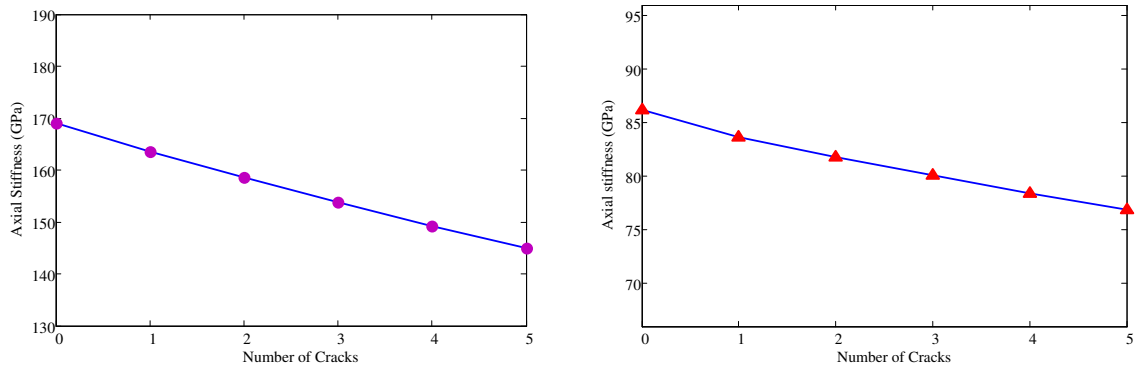

(a) (b)

Figure 12. The results of micromechanics approach: (a) Axial stiffness of silicon layer, (b) Axial stiffness of bimorph

The results of micromechanics approach show that by increasing the number of cracks in the mid-layer both the axial stiffness of mid-layer and axial stiffness of the bimorph piezoelectric energy harvester decreases. The obtained strain energy and the resultant axial stiffness from the finite element analysis for each case are shown in Table 4. The strain energy and the axial stiffness of undamaged structure and damaged structure with different number of cracks in the mid-layer from 1 to 5 are also shown in Figure 13.

Table 4: Calculated strain energy and axial stiffness from finite element analysis

Case	undamaged	1 crack	2 cracks	3 cracks	4 cracks	5 cracks
Total Strain Energy (mJ)	0.597	0.606	0.614	0.623	0.632	0.639
Axial Stiffness (GPa)	80.596	79.431	78.334	77.205	76.106	75.290

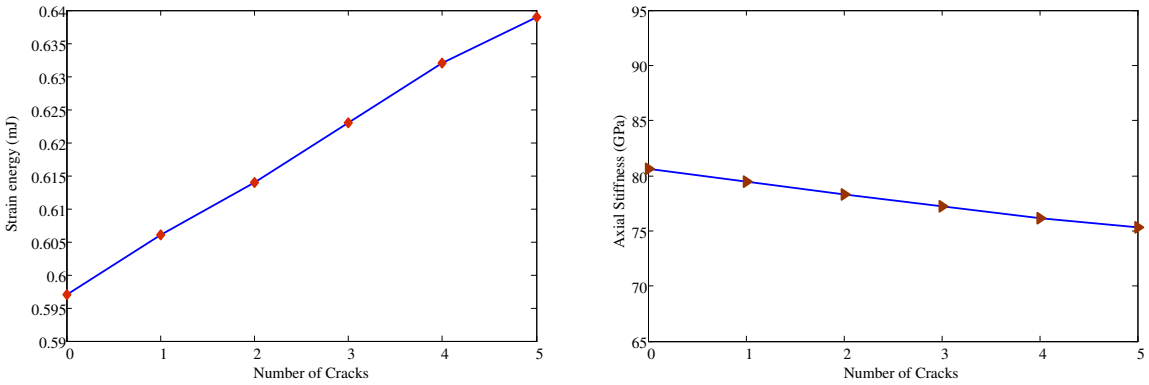

(a) (b)

Figure 13: The results of FEA: (a) Strain energy of bimorph , (b) Axial stiffness of bimorph

It can be observed from finite element analysis that by increasing the number of cracks in the mid-layer of the bimorph piezoelectric energy harvester, the strain energy increases, while its axial stiffness decreases. Comparing the results of stiffness reduction from the micromechanics approach and from the finite element analysis indicates that the theoretical model is very accurate and can be used for further analysis. The effect of silicon layer thickness on the natural frequency of the bimorph piezoelectric energy harvester is shown in Figure 14. Also the natural frequency of the structure is shown in Figure 15. The obtained results demonstrate that as the thickness of the middle layer increases, the natural frequency of the bimorph also increases. As it is expected, by increasing the number of cracks, the natural frequency decreases, which is a logical result due to stiffness reduction of the bimorph energy harvester.

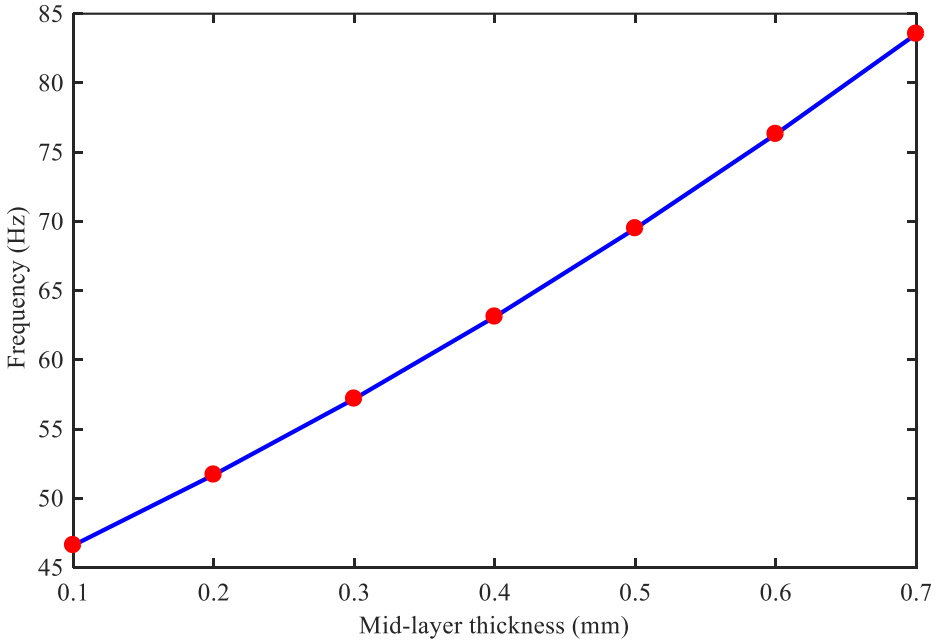

Figure 14: Effect of the mid-layer thickness on the Natural Frequency

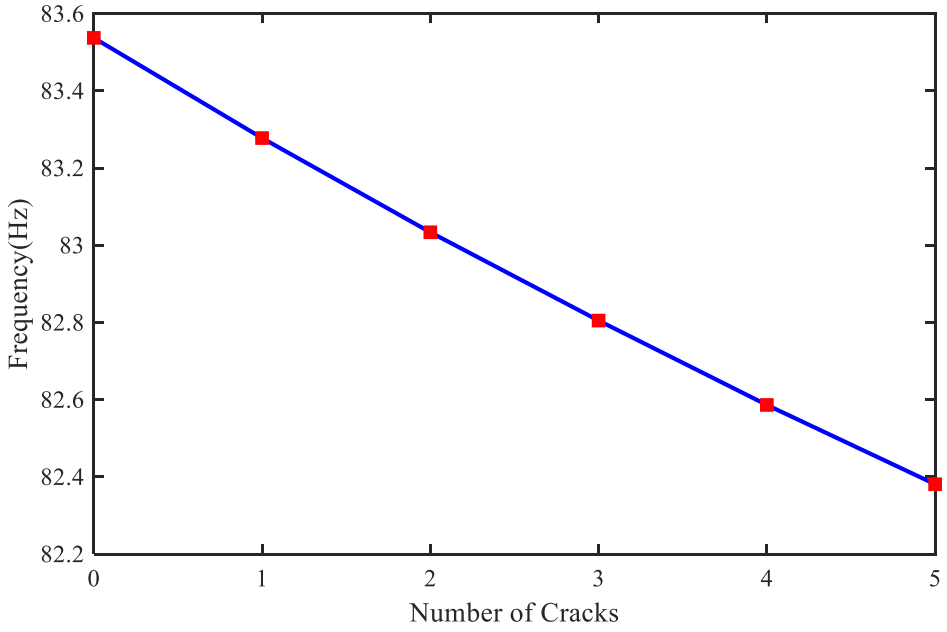

Figure 15: Effect of different mid-layer crack numbers on the Natural Frequency

The output electrical power and voltage for different crack numbers from analytical method are shown in Figure 16 and Figure 17, respectively. Also, the output voltage versus excitation frequency for different crack numbers from finite element analysis is shown in Figure 18 and Figure 19. The predicted output voltage from analytical method is in a good agreement with the finite element analysis results for

propagation of the transverse cracks. In both cases, it is shown that increasing the number of cracks will increase the output voltage with an approximate rate of 0.2 %.

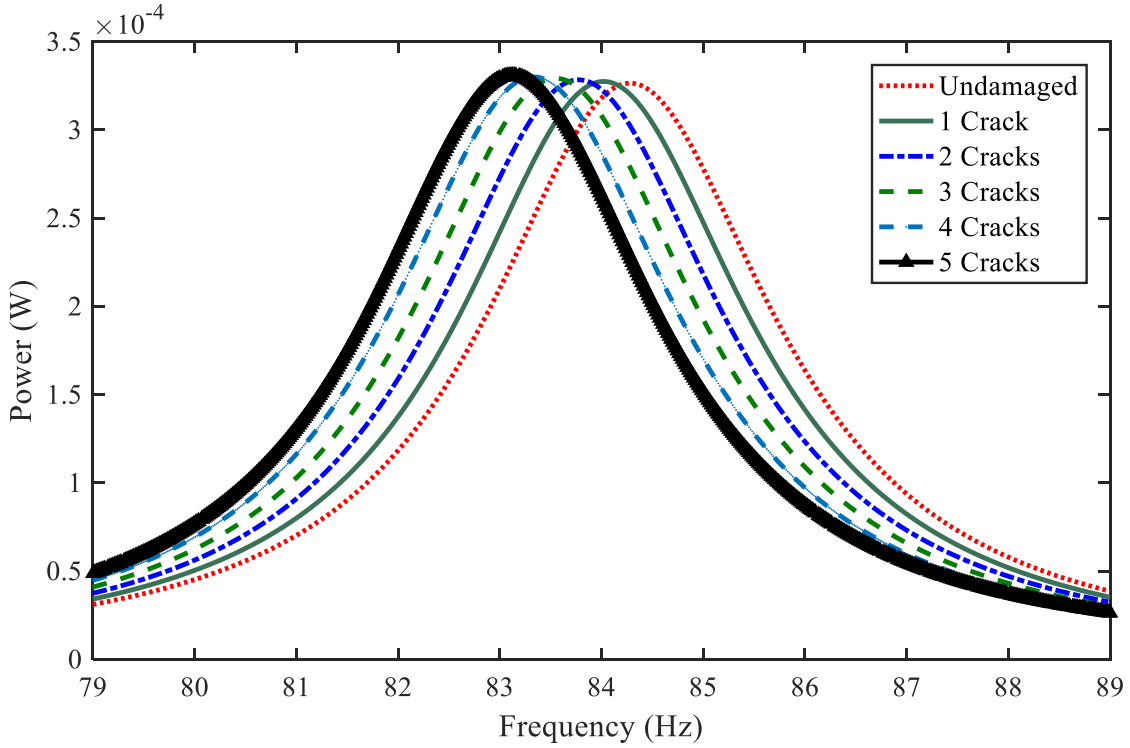

Figure 16: Effect of mid-layer cracks on the Output power from analytical method

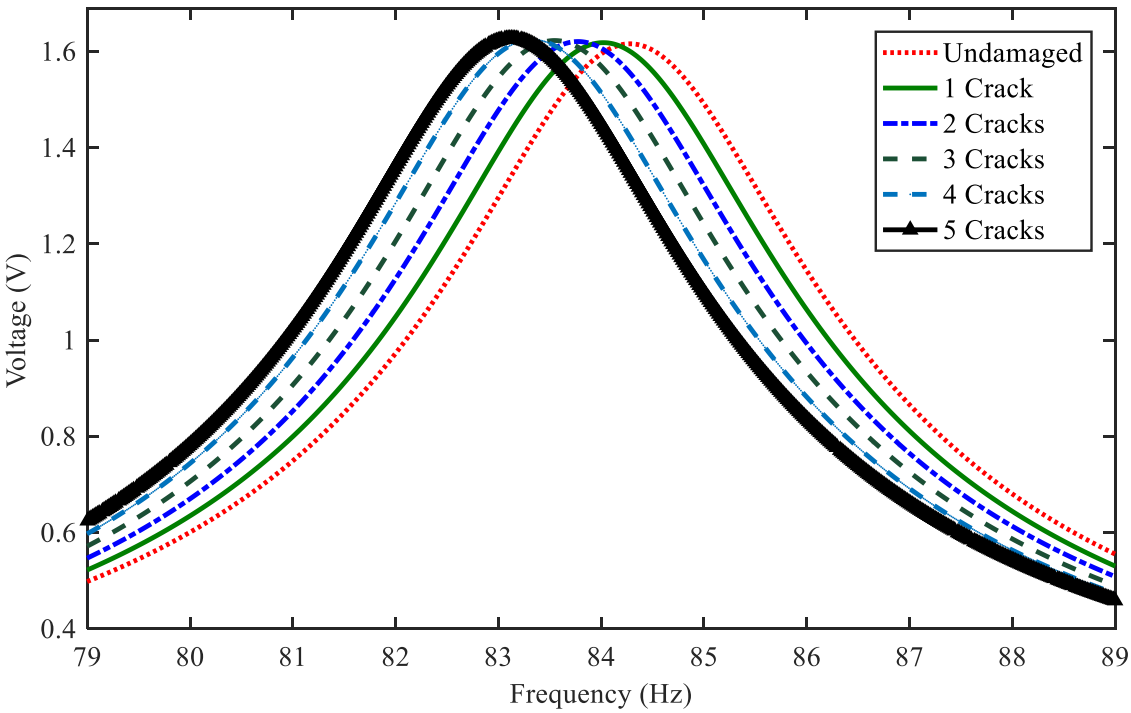

Figure 17: Effect of mid-layer cracks on the Voltage from analytical method

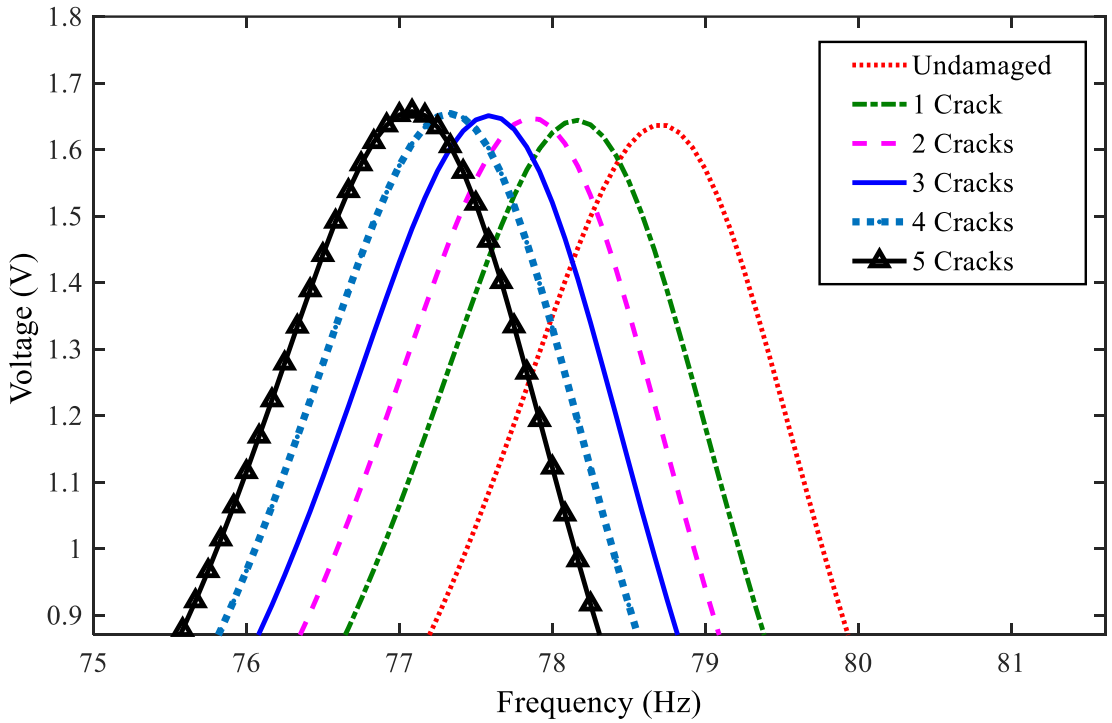

Figure 18: Effect of mid-layer cracks on the Voltage from finite element analysis

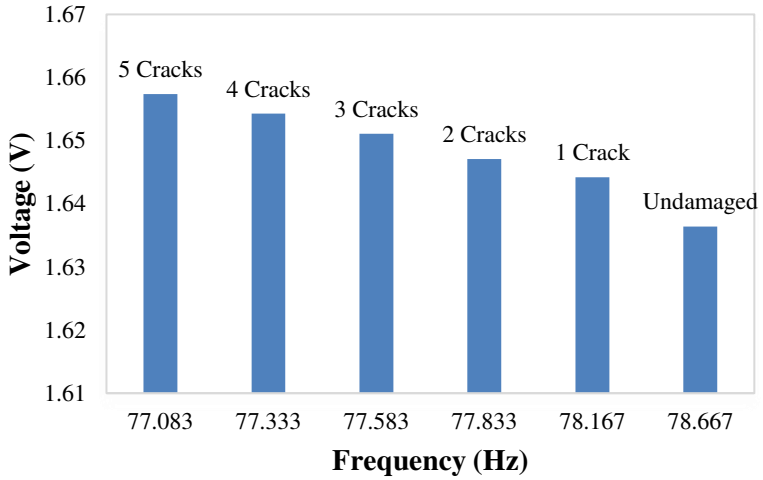

Figure 19: Voltage-Frequency for cracks in the mid-layer of piezoelectric bimorph from FEA

As it can be seen by increasing the number of cracks in the mid-layer of bimorph, the natural frequency of bimorph piezoelectric energy harvester decreases while the voltage and output power increases. Effect of different numbers of mid-layer crack on the Phase angle and Impedance amplitude of the bimorph energy harvester can be seen in Figure 20 and Figure 21, respectively. It is shown that the impedance amplitude will increase by increasing the number of cracks while the phase angle decreases which show other signs of damages in such devices.

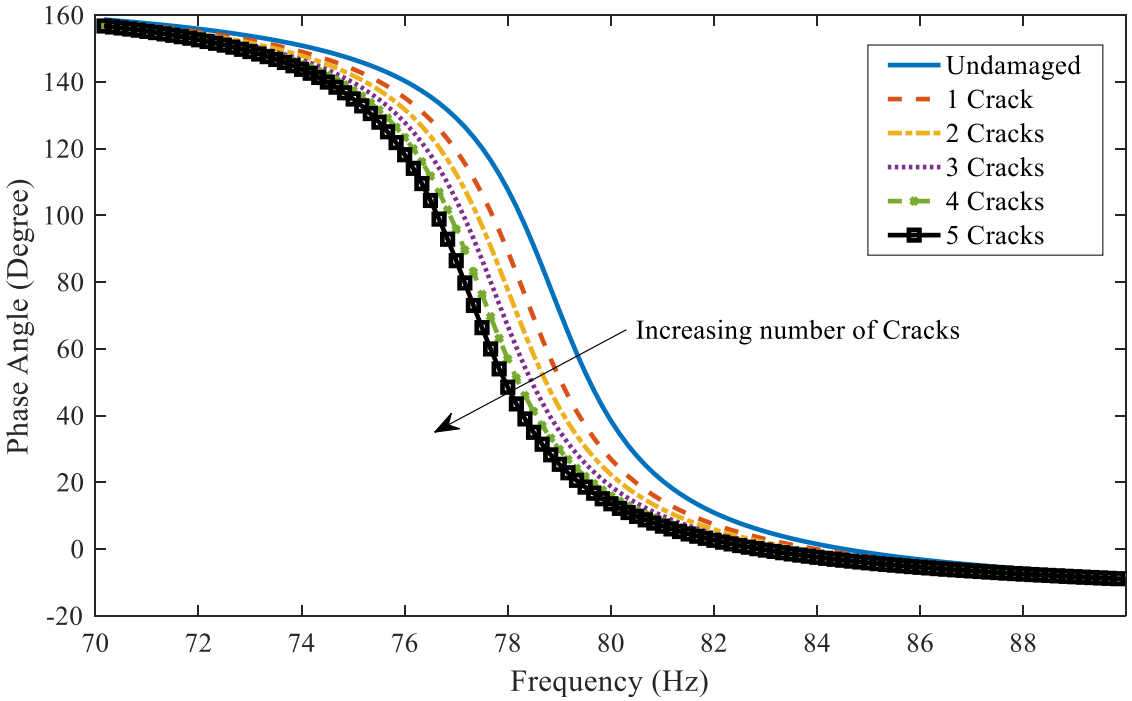

Figure 20: Effect of different mid-layer crack numbers on the Phase Angle

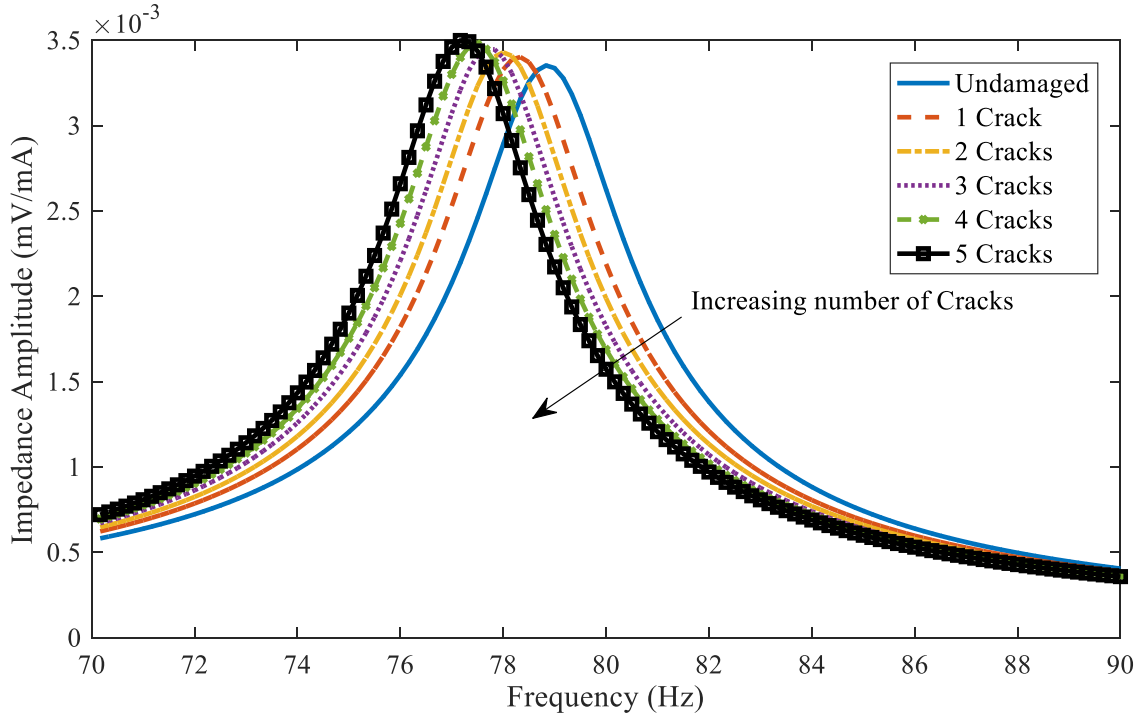

Figure 21: Effect of different mid-layer crack numbers on the Impedance Amplitude

7- Conclusions

This paper presents a semi-analytical solution for analysis of transverse cracks in the mid-layer of bimorph piezoelectric energy harvester for serial and parallel configuration that has been investigated for the first time. The novelty is mainly due to the method by considering both the stiffness reduction and changes in the capacitance of the structure as well as finding of the research. By this research, new physical insights have gained that have not been reported before. These cracks cause a reduction in the structural stiffness as expected. However, in the worst case they could also change the capacitance of the bimorph. By increasing the cracks number in the mid-layer of bimorph, the stiffness, equivalent circuit and the equivalent capacitance changes accordingly. So in this case, if the electric field forms inside the crack, in addition to stiffness reduction, the electric field inside the crack may also affect the output electrical power. For this purpose, after deriving mechanical and electrical coupled differential equations and solving the obtained equations, two methods including micro-meso approach and finite element-fracture mechanics analyses are used to calculate the stiffness reduction of the structure. In addition to stiffness reduction, the formation of electric field inside the crack regarding to serial or parallel connection may also affect the output electrical power. The changes in the equivalent circuit of the piezoelectric energy harvester and the equivalent capacitance of each part including piezoelectric layer and crack section have been investigated and it is shown that the performance of the device has been affected by stiffness reduction. The voltage and output power of the piezoelectric energy harvester with crack faults is increased which is the sign of device failure. The results demonstrate that the output power is more affected by stiffness reduction. The changes in the equivalent capacitance and the probable formation of electrical field inside the transverse cracks have negligible effects in the output power compared to stiffness reduction. The experimentally validated methods have been used for the calculation of both the stiffness reduction and output voltage and power. In general, regarding the acceptable agreement between the presented results of the analytical model with numerical results, the present study proposed a reliable approach for mid-layer damage analysis of bimorph piezoelectric energy harvesters, which can be employed as a method for damage prediction based on the performance of these kind of harvesters.

References

1. U. Aridogan, I. Basdogan, A. Erturk, Analytical modeling and experimental validation of a structurally integrated piezoelectric energy harvester on a thin plate. Smart Mater Struct 2014; 23: 45039. https://doi.org/10.1088/0964-1726/23/4/045039.

2. A.G. A. Muthalif, N.H.D. Nordin, Optimal piezoelectric beam shape for single and broadband vibration energy harvesting: Modeling, simulation and experimental results, Mech Syst Signal Process 2015; 54-55: 417–426. https://doi.org/10.1016/j.ymssp.2014.07.014.
3. F.K. Shaikh, S. Zeadally, Energy harvesting in wireless sensor networks: A comprehensive review, Renew. Sustain. Energy Rev 2016; 55: 1041–1054. https://doi.org/10.1016/j.rser.2015.11.010.
4. C. Wei, X. Jing, A comprehensive review on vibration energy harvesting: Modelling and realization, Renew. Sustain. Energy Rev 2017; 74: 1–18. https://doi.org/10.1016/j.rser.2017.01.073.
5. S. Ravi, A. Zilian, Simultaneous finite element analysis of circuit-integrated piezoelectric energy harvesting from fluid-structure interaction, Mech Syst Signal Process 2019; 114: 259–274. https://doi.org/10.1016/j.ymssp.2018.05.016.
6. Johnson TJ, Charnegie D, Clark WW, Buric M, Kusic G., Energy harvesting from mechanical vibrations using piezoelectric cantilever beams, Smart Mater Struct: damping and isolation 2006; 61690D. https://doi.org/10.1117/12.659466.
7. Anderson TA, Sexton DW., A vibration energy harvesting sensor platform for increased industrial efficiency, In: Smart structures and materials 2006: sensors and smart structures technologies for civil, mechanical, and aerospace systems, proc. of the SPIE 2006; 6174: 621–629. https://doi.org/10.1117/12.659586
8. Erturk A and Inman DJ, A distributed parameter electromechanical model for cantilevered piezoelectric energy harvesters, J Vib Acoust: Transactions of the ASME 2008; 130: 041002. https://doi.org/10.1115/1.2890402.
9. A. Abdelkefi, N. Barsallo, L. Tang, Y. Yang, M. R. Hajj, Modeling, validation, and performance of low-frequency piezoelectric energy harvesters, J Intell Mater Syst Struct 2013; 25: 1429-1444. https://doi.org/10.1177/1045389X13507638.
10. Y. Bai, P. Tofel, Z. Hadas, J. Smilek, P. Losak, P. Skarvada, R. Macku, Investigation of a cantilever structured piezoelectric energy harvester used for wearable devices with random vibration input, Mech Syst Signal Process 2018; 106: 303–318. https://doi.org/10.1016/j.ymssp.2018.01.006.
11. X. Li, D. Upadrashta, K. Yu, Y. Yang, Y, Analytical modeling and validation of multi-mode piezoelectric energy harvester, Mech Syst Signal Process 2019; 124: 613–631. https://doi.org/10.1016/j.ymssp.2019.02.003.
12. Jun Lei, Yuling Chen, Tinh Quoc Bui, Chuanzeng Zhang, Fatigue crack analysis in piezoelectric specimens by a single-domain BEM, Eng Anal Bound Elem 2019; 104: 71-79. https://doi.org/10.1016/j.enganabound.2019.03.030.
13. Balamonica K, Jothi Saravanan T, Bharathi Priya C, Gopalakrishnan N. Piezoelectric sensor–based damage progression in concrete through serial/parallel multi-sensing technique. Struct Health Monit 2020; 19 (2): 339-356. doi.org/10.1177/1475921719845153.
14. Ahmed Aziz Ezzat, Jiong Tang, Yu Ding. A model-based calibration approach for structural fault diagnosis using piezoelectric impedance measurements and a finite element model. Struct Health Monit 2020; 19(6): 1839-1855. doi.org/10.1177/1475921719901168.

15. Wongi S Na. A portable bolt-loosening detection system with piezoelectric-based nondestructive method and artificial neural networks. Struct Health Monit 2022; 21 (2): 683-694. doi.org/10.1177/14759217211026192.
16. M. Shoaib, N. H. Hamid, A. F. Malik, N. B. Zain Ali, and M. Tariq Jan, A review on key issues and challenges in devices level mems testing, J. Sensors 2016; 2016: 1-14. https://doi.org/10.1155/2016/1639805.
17. Wang B.L., Han J C and Du S Y, Electroelastic fracture dynamics for multilayered piezoelectric materials under dynamic anti-plane shearing, Int J Solids Struct 2000; 37: 5219-5231. https://doi.org/10.1016/S0020-7683 (99)00218-8.
18. Gao C.F., Noda N., Thermal-induced interfacial cracking of magnetoelectroelastic materials, Int J Eng Sci 2004; 42: 1347-1360. https://doi.org/10.1016/j.ijengsci.2004.03.005.
19. H.G. Beom, K.M. Jeong, J.Y. Park, S. Lin, G.H. Kim, Electrical failure of piezoelectric ceramics with a conductive crack under electric fields, Eng Fract Mech 2009; 76: 2399-2407. https://doi.org/10.1016/j.engfracmech.2009.08.004.
20. Zhang T.Y., Gao C.F., Fracture behaviors of piezoelectric materials, Theor Appl Fract Mech 2004; 41: 339-379. https://doi.org/10.1016/j.tafmec.2003.11.019
21. O. Viun, A. Komarov, Y. Lapusta, V. Loboda, A polling direction influence on fracture parameters of a limited permeable interface crack in a piezoelectric bi-material, Eng Fract Mech 2018; 191: 143-152. https://doi.org/10.1016/j.engfracmech.2018.01.024.
22. Jan Sladek, Vladimir Sladek, and Michael Wünsche, Analysis of Cracks in Piezoelectric Solids with Consideration of Electric Field and Strain Gradients, Encyclopedia of Continuum Mechanics, Springer 2020. https://doi.org/10.1007/978-3-662-55771-6_237.
23. Cun-Fa Gao, Christoph H€ausler, Herbert Balke, Periodic permeable interface cracks in piezoelectric materials, Int J Solids Struct 2004; 41: 323-335. https://doi.org/10.1016/j.ijsolstr.2003.09.044.
24. Fang D.N., Liu J.X., Fracture Mechanics of Piezoelectric and Ferroelectric Solids, Springer 2013. https://doi.org/10.1007/978-3-642-30087-5
25. V Govorukha, M Kamlah, V Loboda and Y Lapusta, Interface cracks in piezoelectric materials, Smart Mater Struct 2016; 25: 023001. https://doi.org/10.1088/0964-1726/25/2/023001
26. Aibing Zhang, Baolin Wang, Effects of crack surface electrostatic tractions on the fracture behaviour of magnetoelectric composite materials, Mech Mater 2016; 102: 15-25. https://doi.org/10.1016/J.MECHMAT.2016.08.007.
27. Mojtaba Ayatollahi, Amir Hossein Fartash, Multiple interfacial cracks in dissimilar piezoelectric layers under time harmonic loadings, Fatigue Fract Eng Mater Struct 2018; 42: 466-479. https://doi.org/ 10.1111/ffe.12923.
28. K. H. Nam, I. H. Park, and S. H. Ko, Patterning by controlled cracking, Nature 2012; 485: 221-224. https://doi.org/ 10.1038/nature11002.
29. T. Ikehara and T. Tsuchiya, Crystal orientation-dependent fatigue characteristics in micrometer-sized single-crystal silicon, Microsyst. Nanoeng 2016; 2: 16027. https://doi.org/ 10.1038/micronano.2016.27.
30. D. R. McCarter and R. A. Paquin, Isotropic behavior of an anisotropic material: single crystal silicon, Proc. SPIE 2013; 8837: 883707. https://doi.org/ 10.1117/12.2025770.

31. Shunong Jiang, Xianfang Li, Shaohua Guo, Yuantai Hu, Jiashi Yang and Qing Jiang, Performance of a piezoelectric bimorph for scavenging vibration energy, Smart Mater Struct 2005; 14: 769. https://doi.org/ 10.1088/0964-1726/14/4/036.
32. Y. Liao, H.A. Sodano, Model of a single mode energy harvester and properties for optimal power generation, Smart Mater Struct 2008; 17: 065026. https://doi.org/ 10.1088/0964-1726/17/6/065026.
33. F. Qian, Y. Liao, L. Zuo, P. Jones, System-level finite element analysis of piezoelectric energy harvesters with rectified interface circuits and experimental validation, Mech Syst Signal Process 2021; 151: 107440. https://doi.org/10.1016/j.ymssp.2020.107440.
34. Mohamad Rahmani, Amin Farrokhabadi, Prediction of induced delamination development in [θ/90]s composite laminates using a computational analytical approach, Compos Struct 2018; 203: 903-916. https://doi.org/10.1016/j.compstruct.2018.07.018.
35. Farrokhabadi A, Bahrami H, Babaei R. Predicting the matrix cracking formation in symmetric composite laminates subjected to bending loads, Compos Struct 2019; 223: 110945. https://doi.org/10.1016/j.compstruct.2019.110945.
36. Farrokhabadi A, Hosseini Toudeshky H, Mohammadi B. Damage analysis of laminated composites using a new coupled micro-meso approach. Fatigue Fract Eng Mater Struct 2010; 33: 420-35. https://doi.org/10.1111/j.1460-2695.2010.01456.x
37. P. Han, J. Tian, W. Yan, Handbook of Advanced Dielectric, Piezoelectric and Ferroelectric Materials 2008.
38. Corina Covaci and Aurel Gontean, Piezoelectric Energy Harvesting Solutions: A Review, Sensors 2020; 20: 3512. https://doi.org/10.3390/s20123512.